Precipitation of Intermetallic Phases in 22% Cr Duplex Stainless Weld Metals

The kinetics of intermetallic phase formation in the temperature range 675°–1000°C (1247°–1832°F) and effects on mechanical properties and corrosion resistance.

BY L. KARLSSON, L. RYEN AND S. PAK

ABSTRACT. The effect on corrosion resistance and impact toughness of intermetallic phases, formed in the temperature range of 675°–1000°C (1247°–1832°F), was studied for 22%Cr 9%Ni 3%Mo 0.15%N-type duplex stainless weld metals. R-phase precipitated rapidly below 800°C (1472°F). σ-phase succesively replaced R-phase at 800°C and was the only phase forming at higher temperatures. Minor amounts of χ-phase formed at 800°C and continuous, Cr- and Mo-rich, grain boundary films were found after aging at 675°C. The decrease in impact toughness was most rapid around 900°C (1652°F). Deteroriation of corrosion resistance tnok place most quickly at 700° (1652°F) and 900°C due to formation of R- and σ–phase, respectively. Corrosion resistance and toughness are affected simultaneously above 800°C; whereas, loss of corrosion resistance precedes embrittlement at lower temperatures. A significant decrease of ferrite content or an increase in hardness indicates a lowered corrosion resistance and embrittlement. However, ferrite content or hardness cannot be used to guarantee unaffected properties. Loss of corrosion resistance or embrittlement of the weld metal will not occur if recommended welding procedures are followed.

Introduction

Duplex stainless steels have found widespread use during recent years owing to their competitive combination of properties and price. In particular, the combination of high yield strength, good toughness and very good corrosion resistance in the temperature range –50° to 250°C (–58° to 482°F) is attracting interest. Modern duplex stainless steels also have a good weldability, similar to that of common austenitic grades. A wide, and continuously growing, selection of duplex grades is now available ranging from low-alloy grades to high-alloy super-duplex grades.

A cause of concern during production and use of duplex stainless steels is the formation of intermetallic phases at temperatures above approximately 300°C (572°F). This decomposition of the ferrite phase will impair both corrosion resistance and mechanical properties. Precipitation in duplex and super-duplex stainless steels has been investigated rather thoroughly (Refs. 1–7). Below 500°C (932°F), precipitation reactions are slow and long time embrittlement occurs mainly due to decomposition of ferrite into Fe-rich α and Cr-rich α' (Refs. 2, 8, 9). Reviews of phases forming in the temperature range 600°–1000°C (1112°–1832°F) have recently been published (Refs. 4, 10). In this temperature range, embrittlement is mainly due to formation of σ–phase, but also other intermetallic phases such as R- and χ-phase, as well as carbides and nitrides, have been observed.

Duplex stainless weld metals, intended for use without postweld heat treatments, are overalloyed in Ni to ensure formation of a sufficient amount of austenite. For example, weld metals for the most widely used modern duplex stainless steel, the 22%Cr 5%Ni 3%Mo 0.15%N grade (UNS S31803, W.Nr 1.4462), typically contain 9%Ni. Compared to the base metal, duplex weld metals also have a different ferrite morphology and are less homogeneous. Therefore, the precipitation kinetics of duplex base metals cannot directly be used to predict the behavior of duplex weld metals.

The aging response of duplex weld metals has not been investigated in such detail as for duplex base metals. Kotecki studied σ–phase formation above 1000°C (Ref. 11) and Van Nassau, *et al.*, reports qualitative results for embrittlement in the temperature range 700–1000°C (Ref. 12). A detailed study of the precipitation behavior of a duplex weld metal in the temperature range 400°–600°C was recently performed by Nilsson, *et al.* (Refs. 13, 14). However, no detailed information about precipitation in the temperature range 600° to 1000°C (1112°–1832°F), where most rapid precipitation can be expected during weld-

KEY WORDS

Duplex SS
Weld Metal
Intermetallic Phases
SMAW
Precipitation
Mechanical Properties
Corrosion Resistance
Impact Toughness
Elevated Temperature
Microstructure

L. KARLSSON and S. PAK are with The Esab Group, Esab AB, Göteborg, Sweden. L. Ryen is with Chalmers University of Technology, Department of Physics, Göteborg, Sweden.

Table 1 — Chemical Compositions (wt-%) of Weld Metals[a]

Electrodes	C	Si	Mn	P	S	Cr	Ni	Mo	N	O
OK 67.50	0.022	0.86	0.86	0.017	0.006	22.32	9.68	2.91	0.17	0.07
Exp. rutile	0.018	1.00	0.80	0.021	0.012	23.24	10.30	3.10	0.15	0.09
Exp. basic	0.043	0.72	1.61	0.013	0.011	22.49	9.41	2.84	0.14	0.05

(a) The chemical analyses of the weld metals were determined using an optical emission spectrometer, except for C, O and N, where combustion furnaces were used.

ing was available in the literature.

In the present investigation, the effect on properties of intermetallic phases formed in the temperature interval 675°–1000°C was studied for 22%Cr 9%Ni 3%Mo 0.15%N-type duplex weld metals. The investigation was divided into two parts. In the first part, the kinetics of intermetallic phase formation and its dependence on weld metal composition and elemental distribution was studied (Refs. 15, 16). In the second part, the main object was to clarify the effects of precipitation on mechanical properties and corrosion resistance (Refs. 16, 17). One aim was also to investigate if deterioration of impact toughness and corrosion resistance can be monitored by measuring ferrite content and hardness. The results are compared to the behavior of duplex base metals and are discussed in terms of practical implications on welding.

Experimental

Weld Metals

Three duplex stainless steel weld metals with a nominal composition of 22.5% Cr 9.5%Ni 3%Mo 0.16%N were used as experimental materials. The weld metals were deposited by covered electrodes for shielded metal arc welding (SMAW). One of the weld metals was deposited by standard Esab OK 67.50 electrodes and the other two with experimental electrodes. The Esab OK 67.50 electrode has a rutile type of coating and is intended primarily for welding the duplex 22%Cr 5%Ni 3%Mo 0.15%N steel grade. One of the two experimental electrodes (experimental rutile) was based on the Esab OK 67.50 electrode but designed to give a slightly higher alloyed weld metal. However, the composition was balanced to give the same ferrite content. The second experimental electrode (experimental basic) had a basic type of coating. The chemical compositions of the weld metals are given in Table 1.

Welding Procedures

Welds for mechanical testing and corrosion testing in oxalic acid were deposited by the OK 67.50 electrode. Test welds of 330-mm (13-in.) length were produced by 3.25-mm (1/8-in.) diameter. electrodes in buttered 15-mm (0.6-in.) mild steel plates according to ISO 2560. A stringer bead technique was used to deposit 25 thin weld beads with a rather low heat input (0.6 kJ/mm) and a low maximum interpass temperature of 100°C (212°F). This welding procedure was chosen in order to produce a homogeneous weld metal consisting mainly of regions reheated by subsequent weld passes. The intention was to make the weld susceptible to further heat treatments by producing a "worst case" starting condition with a large fraction of microstructure already subjected to one or more reheating thermal cycles.

Table 2 — Heat Treatments

Electrode	Time	675°C	700°C	800°C	900°C	950°C	1000°C
Electrode	Time						
OK 67.50	1 min		X	X	X		
OK 67.50	5 min			X	X		
OK 67.50	30 min		X	X	X	X	X
OK 67.50	3 h		X	X	X		
Exp. rutile	30 min			X			
Exp. rutile	1 h	X					
Exp. basic	30 min			X			
Exp. basic	1 h	X					

All weld metal specimens for other corrosion tests were prepared from weld pads, deposited by the experimental electrode types. The weld pads, approximately 50 x 50 x 100 mm (2 x 2x 4 in.), were produced by 3.25-mm diameter. electrodes. Around 100 stringer beads were deposited on each pad with a maximum interpass temperature of 150°C (302°F) and a heat input of approximately 0.8 kJ/mm.

Heat Treatments

Heat treatments of impact and corrosion test specimens were performed according to Table 2. The 1- and 5-min heat treatments were made in a weld simulator using rapid resistance heating (≈ 5 s heating up time); whereas, longer heat treatments were performed in a laboratory furnace. All heat treatments were followed by rapid quenching in water.

Microstructural Evaluation

The ferrite content of the weld metals was determined in Ferrite Numbers (FN) using a Magne-Gage instrument (Ref. 18). Overviews of the microstructures were obtained by light optical microscopy. Etching in Murakami's etchant and color etching according to Beraha were used to produce contrast between the ferrite and the austenite and to reveal the presence of precipitates (Ref. 19). More detailed studies of the microstructure were performed by scanning electron microscopy (SEM) combined with microanalysis and by transmission electron microscopy (TEM). Precipitates were identified by electron diffraction and analytical transmission electron microscopy (AEM). In addition, x-ray diffraction analysis of extracted residue was performed in a Guinier-Hägg camera for some heat treatments.

Thin foils for transmission electron microscopy were prepared electrochemically from cross-sections of the weld metals using 15% perchloric acid in methanol. The foils were examined in a Philips EM 300 TEM and in a JEOL 2000FX ATEM equipped with a LINK AN 10 000 unit for energy dispersive x-ray analysis (EDX). Carbon replicas for chemical analysis of extracted particles by AEM were prepared by etching in 12.5 g $CuCl_2$ dissolved in 50 mL ethanol and 30 mL hydrochloric acid. This etchant was also used to prepare polished surfaces for SEM studies. At least five particles were analyzed by AEM for each type of particle and heat treatment.

The volume fractions of precipitates in the OK 67.50 weld metal were estimated by a combination of image analysis of SEM images, from the decrease in ferrite content and from information from

Fig. 1 — Microstructure of duplex weld metal in as-welded condition. Allotriomorphic grain boundary austenite and Widmanstätten type austenite (white) are seen in the colored ferrite. 250X.

optical and TEM micrographs. Rough estimates of precipitate volume fractions in the experimental weld metals were obtained by comparing with micrographs from the OK 67.50 weld metal.

Mapping of the elemental distribution of carbon and nitrogen was made using secondary ion mass spectroscopy (SIMS). In preparation for SIMS analysis, the surfaces were mechanically polished and carefully cleaned. The analyses were performed in a Cameca IMS 3F/4F instrument using Cs+ as primary ions and the negatively charged secondary ions emitted from the surface to obtain mass resolved ion images.

Mechanical Testing

The impact toughness was determined for standard Charpy V-notch impact specimens (10 x 10 x 55 mm/0.4 x 0.4 x 2.2 in.) with the notch located at the center of the weld metal. Three specimens were tested at room temperature for each heat treatment. Hardness testing was performed using the Vickers method with a 10-kg load.

Corrosion Testing

Fractured impact test specimens were corrosion tested by electrochemical etching in oxalic acid. The specimens were embedded in epoxy, exposing only the fracture surface. The fracture surfaces were ground flat removing enough material to avoid any effect of deformation from impact testing. Etching was performed in 10% oxalic acid at room temperature, with a current of 1 A/cm^2 (6.5 A/in.^{2}) and an etching time of 30 s. The resulting etched structures were then evaluated by light optical microscopy.

The resistance to intergranular corrosion of the weld metals deposited with the experimental electrodes was evaluated using the Streicher test (ASTM A262 practice B) and the Huey test (ASTM A262 practice C) (Ref. 20). Two specimens in each of the following conditions were tested: as–welded, heat treated 1 h at 675°C (1247°F) or 30 min at 800°C. All surfaces were wet ground using 120-grit SiC-paper before testing.

Results

Microstructure

All three weld metals had a typical duplex weld metal microstructure in the as–welded condition. The structure consisted of primary ferrite grains with allotriomorphic austenite precipitated on the grain boundaries, and with austenite growing in a Widmanstätten manner from the grain boundary austenite into the ferrite grains — Fig. 1.

The only inclusions present after

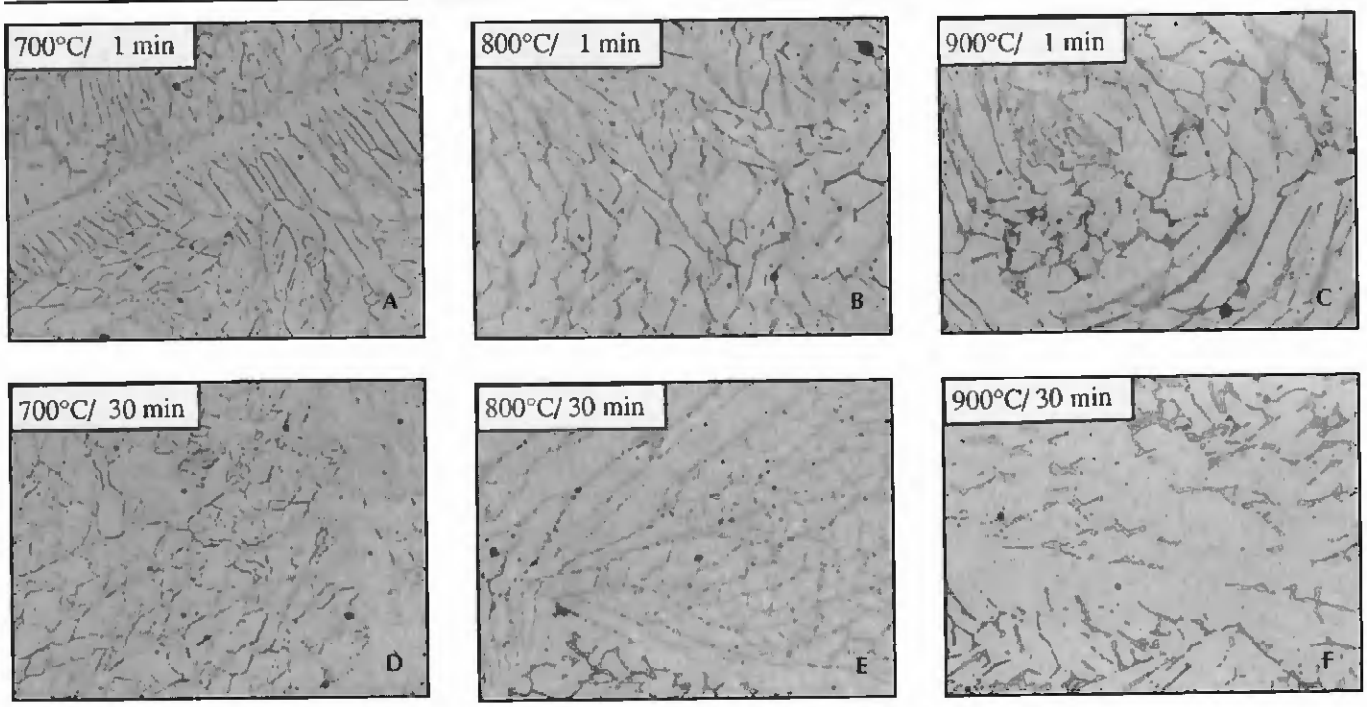

Fig. 2 — Light optical micrographs showing the microstructure of the OK 67.50 weld metal after 1 or 30 min aging at 700°, 800° or 900°C. Austenite is white, ferrite is gray and precipitates are dark. Small precipitates are visible in the ferrite and at ferrite/austenite phase boundaries after 30 min aging at 700° or 800°C. Larger precipitates are present after heat trreatment at 900°C and after 30 min aging at 800°C.

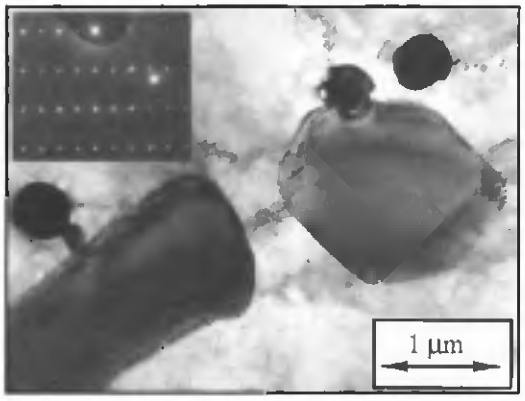

Fig. 3 — Bright field TEM image and (101) diffraction pattern from σ-phase particles formed in the OK 67.50 weld metal during 3 h aging at 900°C.

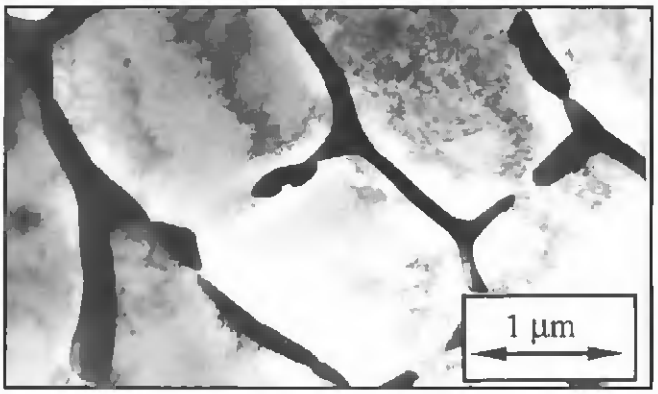

Fig. 4 — σ–phase (dark phase) network found in the OK 67.50 weld metal after 3 h aging at 800°C. Bright field TEM micrograph.

welding were microslag particles, likely very stable complex oxides and silicates, which always form during welding. However, other precipitates formed in the ferrite and at ferrite/austenite phase boundaries during heat treatment. Basically two morphologies of precipitates appeared. Small precipitates dominated after aging at 675° or 700°C and occurred frequently up to 30 min aging at 800°C. Larger precipitates, that replaced the ferrite after long aging times, were in the majority after 3 h aging at 800°C and the only type seen after heat treatment at and above 900°C — Fig. 2. Some large precipitates were also found after 3 h heat treatment at 700°C. The general precipitation behavior was similar for all three weld metals. However, precipitation was less extensive in the experimental basic weld metal than in the other two weld metals, in particular after aging at 800°C (Ref. 15).

Precipitates

Three different intermetallic phases were identified in the heat treated weld metals: tetragonal σ-phase (a = 0.879 nm, c = 0.454 nm (Ref. 21)), rhombohedral R-phase (a = 1.090 nm, c = 1.934 nm (Ref. 22)), and cubic χ-phase (a = 0.892 nm (Ref. 23)). All three types formed in the ferrite or at ferrite/austenite phase boundaries. A few precipitates identified as cubic $M_{23}C_6$ carbides were also found in the experimental weld metals after aging at 675°C. However, no nitrides were identified, neither by TEM nor by x-ray diffraction analysis on extracted residue.

σ-Phase

σ-phase was the intermetallic phase occurring most frequently in largest volume fractions and the only type found at all heat treatment temperatures. It formed rather large, elongated particles in the ferrite, giving an even contrast in TEM — Fig. 3. After long aging times, the ferrite was replaced almost completely by σ-phase, forming an almost continuous network — Fig. 4. Since the larger particles seen in optical micrographs for the 700°–900°C heat treatments mainly are σ-phase, it was assumed that the precipitates formed at 950° and 1000°C were also σ-phase.

R-Phase

R-phase was found after heat treatment at 675°, 700° or 800°C. The R-phase particles had a characteristic irregular shape and uneven, usually speckled contrast in TEM (Fig. 5). R-phase precipitated mainly at ferrite/austenite phase boundaries, but also to some extent inside the ferrite grains — Fig. 6. Most of the R-phase appeared as small particles (≈0.01-0.1 µm), but also larger R-phase particles were found in the OK 67.50 weld metal after aging for 3 h at 700°C or for 30 min at 800°C — Fig. 5. R-phase was the dominating phase after aging for 3 h at 700°C and approximately the same volume fractions of R- and σ-phase were found after 5 or 30 min aging at 800°C. However, σ-phase had largely replaced R-phase after 3 h at 800°C — Fig. 7. A comparison between light optical and

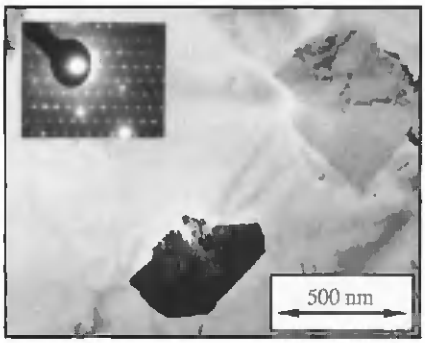

Fig. 5 — Bright field TEM image and (1010) diffraction pattern from large R-phase particles in the OK 67.50 weld metal aged 30 min at 800°C.

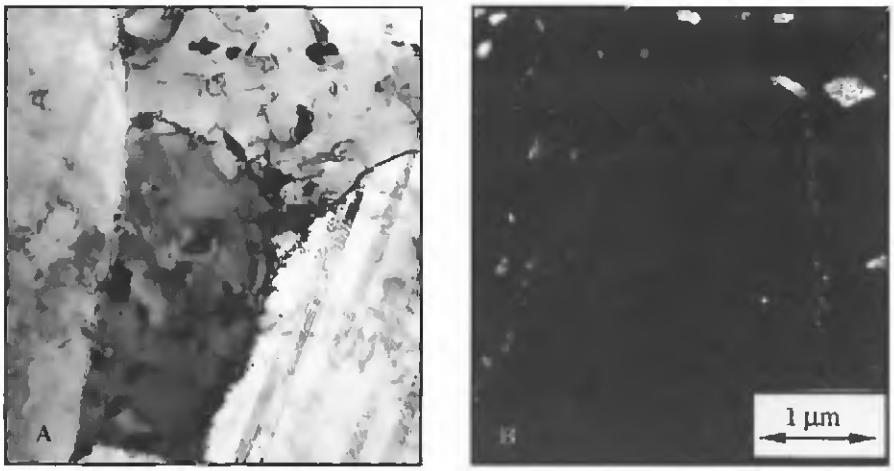

Fig. 6 — Bright and dark field TEM images showing R-phase particles in ferrite and at ferrite/austenite boundaries in the rutile experimental weld metal aged for 1 h at 675°C.

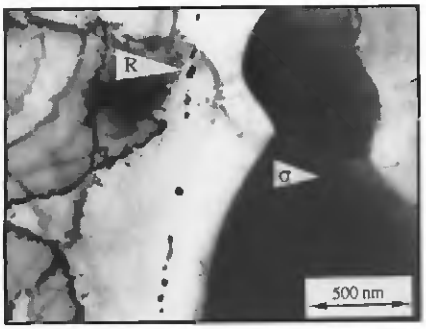

Fig. 7 — TEM micrograph of precipitates in the OK 67.50 weld metal aged for 3 h at 800°C. Large σ-phase particles have replaced ferrite and small R-phase remain in austenite at previous position of ferrite/austenite boundary.

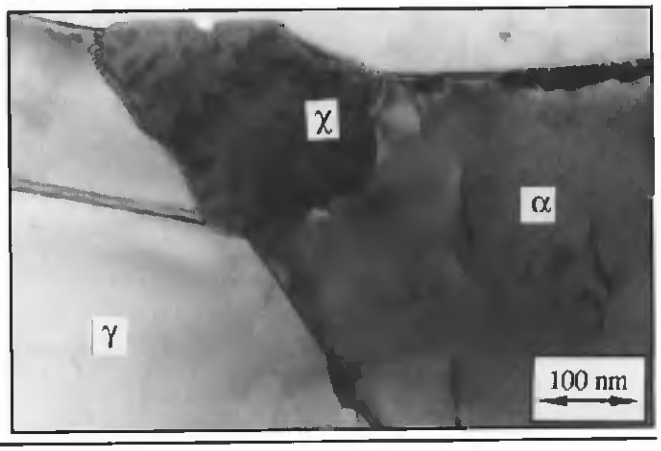

Fig. 8 — Bright field TEM image of χ-phase particle in experimental basic weld metal aged for 30 min at 800°C.

TEM micrographs shows that the majority of small precipitates seen in optical micrographs are R-phase.

χ-Phase

χ-phase precipitates having a rounded, often rectangular shape, were found in the basic experimental weld metal aged for 30 min at 800°C — Fig. 8. Small amounts of χ-phase were also found in the OK 67.50 weld metal specimens heat treated at 800°C for 5 min. The typical size of the precipitates was the same (≈ 0.5 μm) for both heat treatments. No χ-phase was identified after heat treatment at any other temperature.

Comparison between Weld Metals

The results of the TEM investigations for the OK 67.50 Weld Metal are summarized in Table 3. σ-phase was the only phase found at all heat treatment temperatures, R-phase occurred up to 800°C and χ-phase was occasionally found after aging at 800°C.

The same intermetallic phases were identified in the experimental weld metals as in the OK 67.50 weld metal. However, a few $M_{23}C_6$ carbides were also found after aging at 675°C. The precipitates present in largest volume fractions in both experimental weld metals were R-phase after aging at 675°C and R- and σ-phase after aging at 800°C. Traces of σ-phase were found after the 675°C heat treatment. χ-phase was only identified in the basic experimental weld metal after aging at 800°C. The main difference between the two experimental weld metals was the more extensive precipitation of intermetallic phases in the rutile weld metal, in particular after aging at 800°C. The number of carbides seemed to be slightly higher in the basic weld metal. It should be made clear, though, that the carbides occurred very sparsely and could be found only when larger regions were scanned using the carbon replica technique.

Grain Boundary Films

An interesting and unexpected feature was the presence of thin films on several ferrite/austenite boundaries. The films were found in the experimental weld metals heat treated at 675°C. They appeared to be continuous and gave a speckled contrast in TEM — Figs. 9, 10. Larger grain boundary precipitates were sometimes present in the films — Fig. 10. The films were too thin to obtain useful structural information from electron diffraction.

Volume Fractions of Precipitates

The phase present in largest volume fractions in the OK 67.50 weld metal is clearly σ-phase at temperatures above 800°C. R-phase is the dominating precipitate type for short aging times below 800°C. However, R-phase is succesively replaced by σ-phase after longer aging times The results are summarized in a

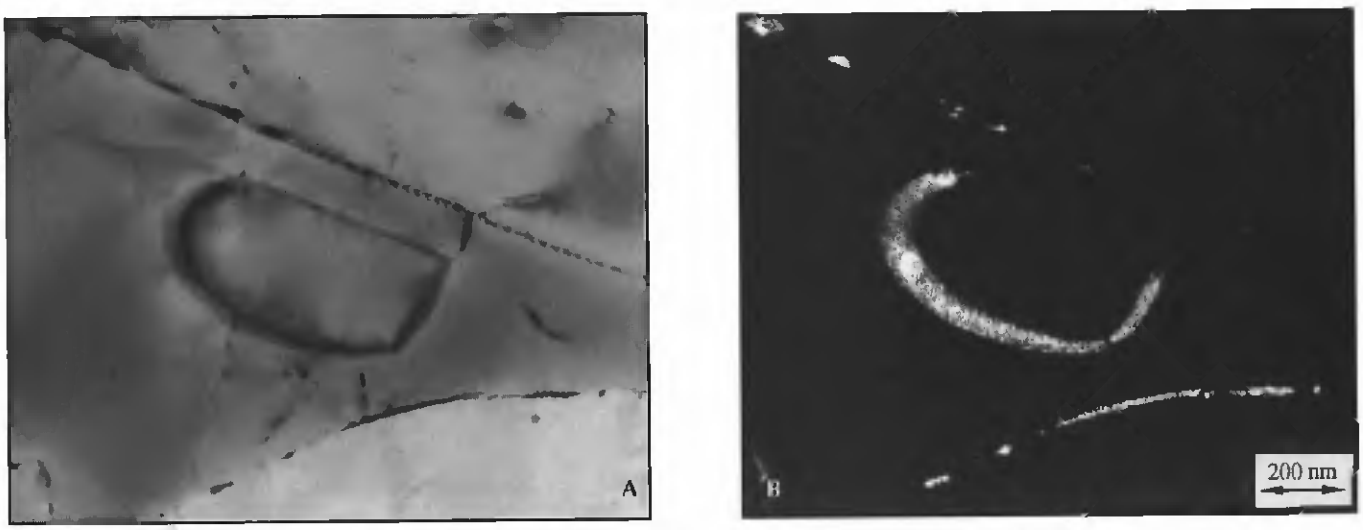

Fig. 9 — Grain boundary films formed at many ferrite/austenite boundaries at 675°C. Bright and dark field TEM images of the basic experimental weld metal aged for 1 h at 675°C.

TTT-diagram for R- and σ-phase in Fig. 11.

An estimate of precipitate volume fractions in the experimental rutile weld metal gives a good agreement with the TTT-diagram — Fig. 11. However, the TTT-diagram clearly overestimates the volume fractions for the basic weld metal although the general precipitation behavior is the same.

Chemical Composition of Precipitates

A summary of the results from AEM analysis of precipitates and grain boundary films extracted on carbon replicas and from SEM-EDX analysis is given in Table 4 (see also Ref. 16). The σ-phase was rich in Cr but only slightly enriched in Mo; whereas, R-phase had a high Mo-content and a Cr-content similar to the average weld metal composition. χ-phase had an intermediate composition compared to R- and σ-phase.

The σ-phase in the experimental weld metals, analyzed by SEM-EDX, had a higher Fe- and Ni-content and a lower Mo- and Cr-content than σ-phase in the OK 67.50 weld metal. However, some influence of the surrounding matrix during SEM-EDX analysis cannot be ruled out due to the small precipitate size. Therefore, no conclusion can be made with regard to the differences in composition of σ-phase for the three weld metals.

Three things can be noted regarding R-phase. Firstly, smaller R-phase particles are significantly richer in Mo and contain less Cr than large R-phase particles, for comparable aging temperatures. Secondly, the Cr content of small R-phase particles decreases; whereas, the Mo-content appears to increase with increasing aging temperature. Thirdly, the Cr-content of small R-phase particles seems to decrease with longer aging times.

The small thickness of the grain boundary films, extracted from the experimental basic weld metal heat treated at 675°C, and the presence of particles in the films made it difficult to determine the composition with great accuracy. It is clear, though, that the film is rich in Cr and Mo and poor in Ni. The composition was similar to that of the small R-phase particles in the same specimen — Table 4.

Elemental Distribution

Metallic Elements

The compositions of ferrite and austenite were compared for the experimental weld metals in the as welded condition by SEM-EDX studies. The well-known enrichment of elements such as Cr and Mo to the ferrite and of Ni to the austenite was clear for both weld metals — Fig. 12. However, the difference in composition between the ferrite and austenite was larger for the rutile than for the basic weld metal —Table 5. In particular, the enrichment of Cr and Mo to the ferrite was larger for the rutile experimental weld metal.

C and N

Secondary ion mass spectroscopy (SIMS) was used to map the elemental distribution in the experimental weld metals in the as-welded condition and after heat treatment for 1 h at 675°C. The lateral resolution of the instrument used is on the order of 1 μm, which is sufficient to differentiate between ferrite and austenite in duplex weld metals but does not permit individual small precipitates to be resolved. However, it is nevertheless often possible to reveal the presence of small precipitates, for example carbides or nitrides, from variations in intensity in SIMS images.

The distribution of C and N was very

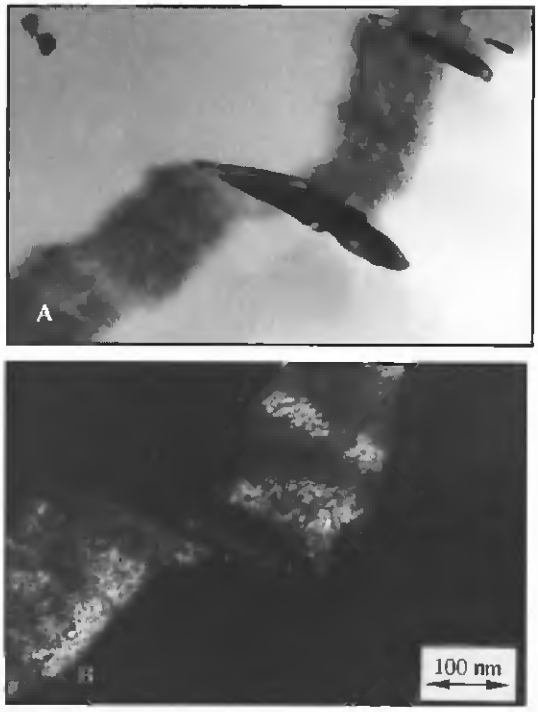

Fig. 10 — Bright and dark field TEM images showing precipitates and speckled contrast of film at a ferrite/austenite phase boundary. Basic experimental weld metal aged for 1 h at 675°C.

Table 3 — Precipitate Types and Typical Sizes for the OK 67.50 Weld Metal

	σ-phase		R-phase		χ-phase	
Heat treatment	Found?	Size (μm)	Found?	Size (μm)	Found?	Size (μm)
700°C/3 h	⊗	0.1 × 0.4	⊗	0.01–0.1		
			⊗	≈0.5		
800°C/5 min	⊗	0.4 × 1.5	⊗	0.05–0.3	⊗	0.1–0.3
800°C/30 min	⊗	0.6 × 1.5	⊗	0.08–0.3		
			⊗	≈0.5		
800°C/3 h	⊗	1.0 × 2.5	⊗	0.05		
900°C/1 min	⊗	0.4 × 1.0				
900°C/5 min	⊗	0.6 × 1.5				
900°C/30 min	⊗	1.0 × 2.5				
900°C/3 h	⊗	2.0 × 5.0				

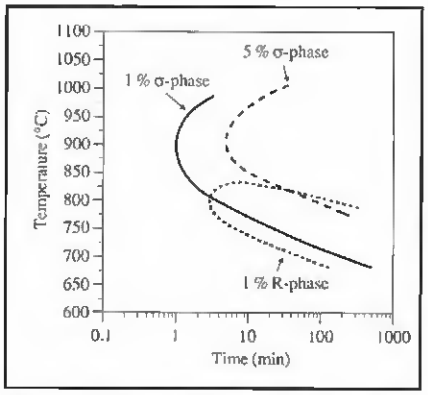

Fig. 11 — TTT-diagram for R- and σ-phase precipitation in 22Cr-9Ni-3Mo-0.15N type duplex weld metal.

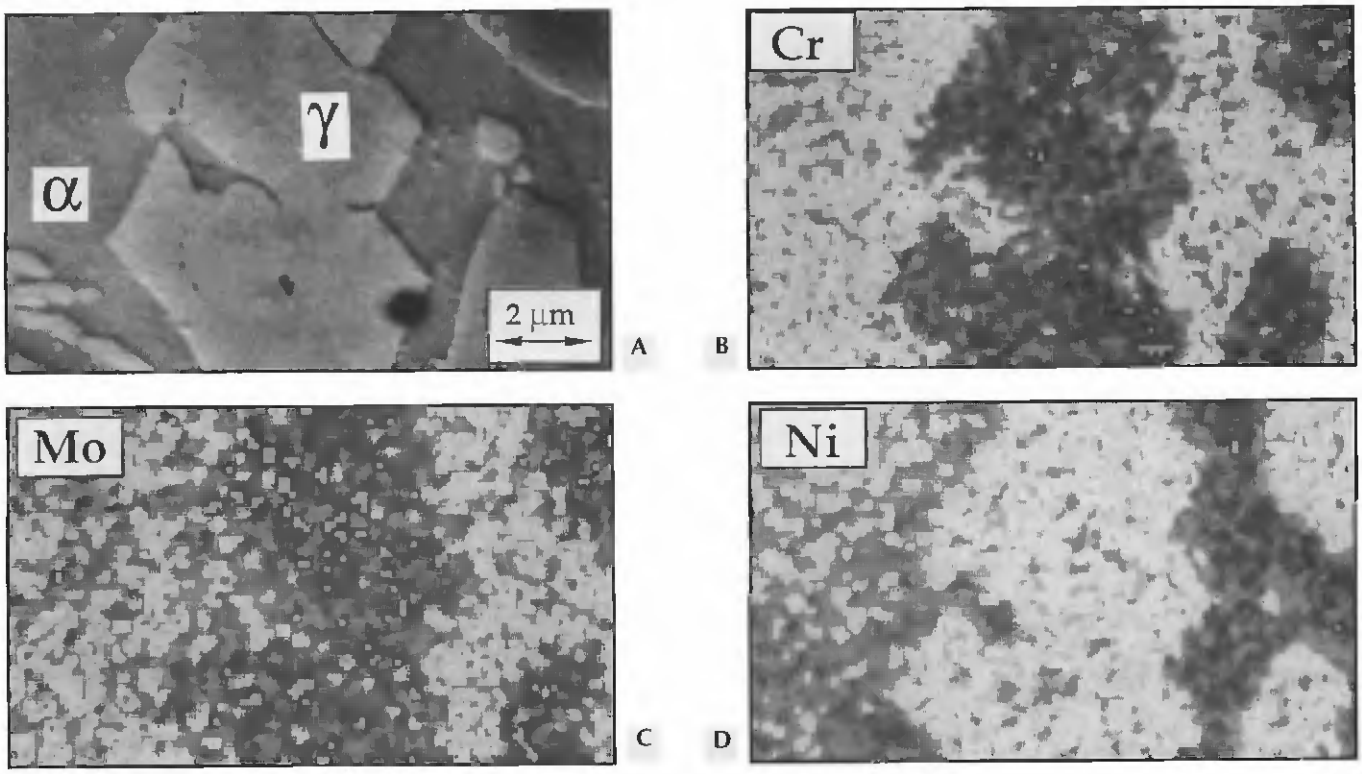

Fig. 12 — Concentration maps and corresponding SEM micrograph showing the elemental distribution in the OK 67.50 weld metal in as-welded condition. Cr and Mo is enriched to the ferrite (a) and Ni to the austenite (g). Red corresponds to the highest concentration, and blue to the lowest.

Table 4 — Average[a] Chemical Composition of Precipitates in Heat Treated Weld Metals

		Fe	Cr	Ni	Mo	Si
OK 67.50						
σ-phase	800°C/3 h	54.0	34.3	4.1	6.5	1.2
σ-phase	900°C/30 min	55.1	34.8	4.0	5.1	0.9
Small R-phase	700°C/3 h	36.0	21.6	3.5	35.5	3.4
Small R-phase	800°C/5 min	33.2	19.8	3.3	39.2	4.5
Small R-phase	800°C/3 h	37.6	16.4	3.2	38.6	4.1
Large R-phase	700°C/3 h	42.7	26.3	3.7	24.9	2.4
Large R-phase	800°C/30 min	43.4	24.6	3.6	25.8	2.7
x-phase	800°C/5 min	49.3	27.8	3.4	17.8	1.6
Exp. rutile σ-phase[b]	800°C/30 min	59.8	26.3	6.6	5.3	1.2
Exp. basic σ-phase[b]	800°C/30 min	61.5	25.2	6.1	4.3	1.2
Small R-phase	675°C/1 h	33.6	30.0	4.8	27.4	3.0
G.b. film	675°C/1 h	25.9	33.0	3.1	32.7	3.1

(a) The composition is given in wt-% as the mean value for five particles for the OK 67.50 weld metal and for three particles for the experimental weld metals.
(b) SEM-EDX analysis.

Table 5 — Difference in Chemical Composition between Ferrite and Austenite ($C_{ferrite}$-$C_{austenite}$ (wt-%)) for the Experimental Weld Metals

	Cr	Ni	Mo
Experimental rutile	+2.2	−2.4	+1.1
Experimental basic	+0.7	−1.4	+0.4

similar for the two experimental weld metals in both the as-welded condition and after 1 h heat treatment at 675°C. Virtually all C and N appeared to be located within the austenite whereas the signal from the ferrite was very weak — Fig. 13. Furthermore, the intensity within individual grains was even and no indications of carbide or nitride precipitation could be found, neither inside ferrite or austenite grains nor at ferrite/austenite phase boundaries.

Ferrite Content, Hardness and Impact Toughness

The ferrite content, the hardness and the room-temperature impact toughness before and after aging are given in Table 6. The scatter in impact toughness and ferrite content for each heat treatment was small, typically ±2 J and ±2 FN, respectively. However, the variation in hardness was somewhat larger, typically ± 10 HV_{10}.

The ferrite content of the experimental weld metals was slightly higher than

for the OK 67.50 weld metal in the as-welded condition. However, the decrease in ferrite content after aging was similar for all three weld metals. The ferrite content decreased with longer heat treatment times at all temperatures. A significant change of the ferrite content was found within 1 min of aging at 900°C of the OK 67.50 weld metal; whereas, a clear decrease could not be seen until after 3 h at 700°C.

The hardness increased with longer aging times and the highest hardness values were measured after 3 h at 800° and 900°C. Also, at 700°C a clear increase in hardness was found after all heat treatments. However, for this temperature there seemed to be no further increase in hardness after the initial hardness increase.

The changes in impact toughness were most pronounced for long aging times. For example, after 3 h at 800°C, after 30 mins or 3 h at 900°C, and after 30 min at 950°C, all specimens were clearly brittle and the impact toughness had decreased to below 4 J. However, the decrease was much more rapid at higher temperatures. At 700°C embrittlement could not be seen until after 3 h; whereas, a decrease was seen already after 5 min at 800° and 900°C. At 950°C the behavior seems to be similar to that at 900°C; whereas, at 1000°C the impact toughness after 30 min is close to that after 30 min at 800°C. It can also be noted that the impact toughness actually increased, compared to the as-welded condition, for aging times up to 30 min at 700°C and for 1 min aging at 800°C.

Corrosion Testing

Oxalic Acid Etching Test

The dissolution rate in oxalic acid was high for the precipitates compared to that of austenite and ferrite — Fig. 14. This rapid etching of precipitates produced a very distinct contrast in light optical micrographs. Two types of etch structures could be seen in the heat treated weld metals. Small, spot-like localized attacks were taken as indications of the presence of individual small precipitates and larger continuous regions (Fig. 14), suggesting the presence of larger precipitates.

Oxalic acid etch structures of the OK 67.50 weld metal in the as-welded condition and after the 1 and 30 min heat treatments are shown in Figs. 15 and 16. Small precipitates in the ferrite and at ferrite/austenite phase boundaries appear in some regions already after 1 min aging at 700° or 800°C. The number of precipitates is very small after 1 min aging at 800°C but is significant after the 1-min heat treatment at 700°C. Small precipitates are frequent after longer times at 700°C and up to 30 min aging at 800°C. Larger precipitates are the only type after heat treatment at 900°C and are the main type after 3 h aging at 800°C. Large precipitates also appear after 3 h at 700°C and after 5 or 30 min at 800°C. The ferrite is almost completely replaced by rapidly etching precipitates after 3 h aging at 800° or 900°C.

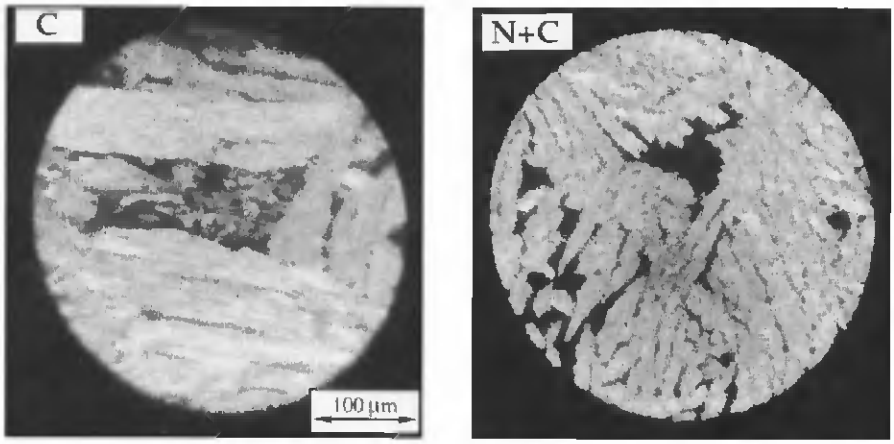

Fig. 13 — SIMS images showing the elemental distribution in the experimental weld metals heat treated for 1 h at 675°C. The very weak signal from the ferrite shows that virtually all C and N is present in the austenite. A — C ditribution in the basic experiemental weld metal; B — C+N distribution in the rutile experiemental weld metal.

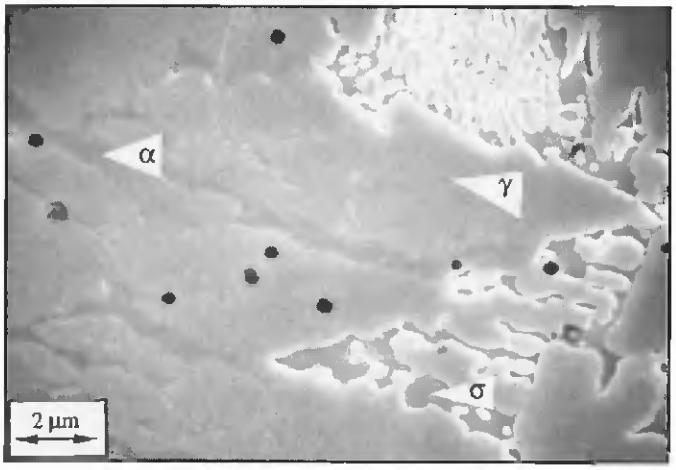

Fig. 14 — SEM micrograph illustrating the different dissolution rates of austenite (γ), ferrite (α) and intermetallic phases during oxalic acid etching. σ-phase is most heavily etched, whereas, austenite is only lightly etched.

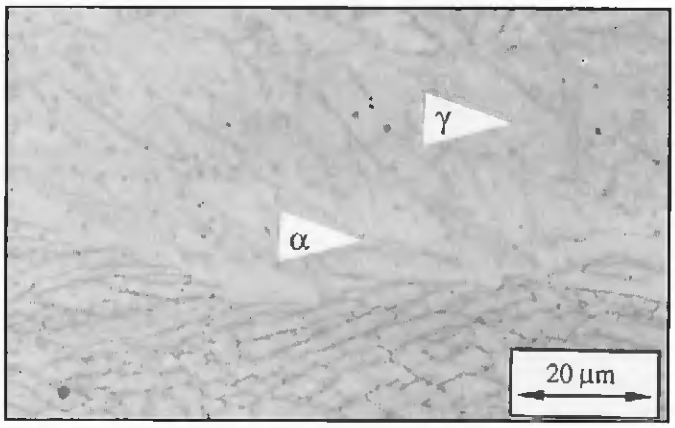

Fig. 15 — Light optical micrograph of the OK 67.50 weld metal in as-welded condition. The ferrite (α) was etched more heavily in oxalic acid than the austenite (γ). No indications of precipitation can be found, but etching at mircoslag inclusions is seen as evenly distributed darker spots.

Streicher and Huey Test

The corrosion rate in the Streicher and Huey tests was higher for the rutile than for the basic experimental weld metal — Table 7. A small difference in corrosion rate was found already in the as-welded condition. This difference was accentuated after heat treatments at 675° or 800°C, giving a corrosion rate of the rutile weld metal almost three times that of

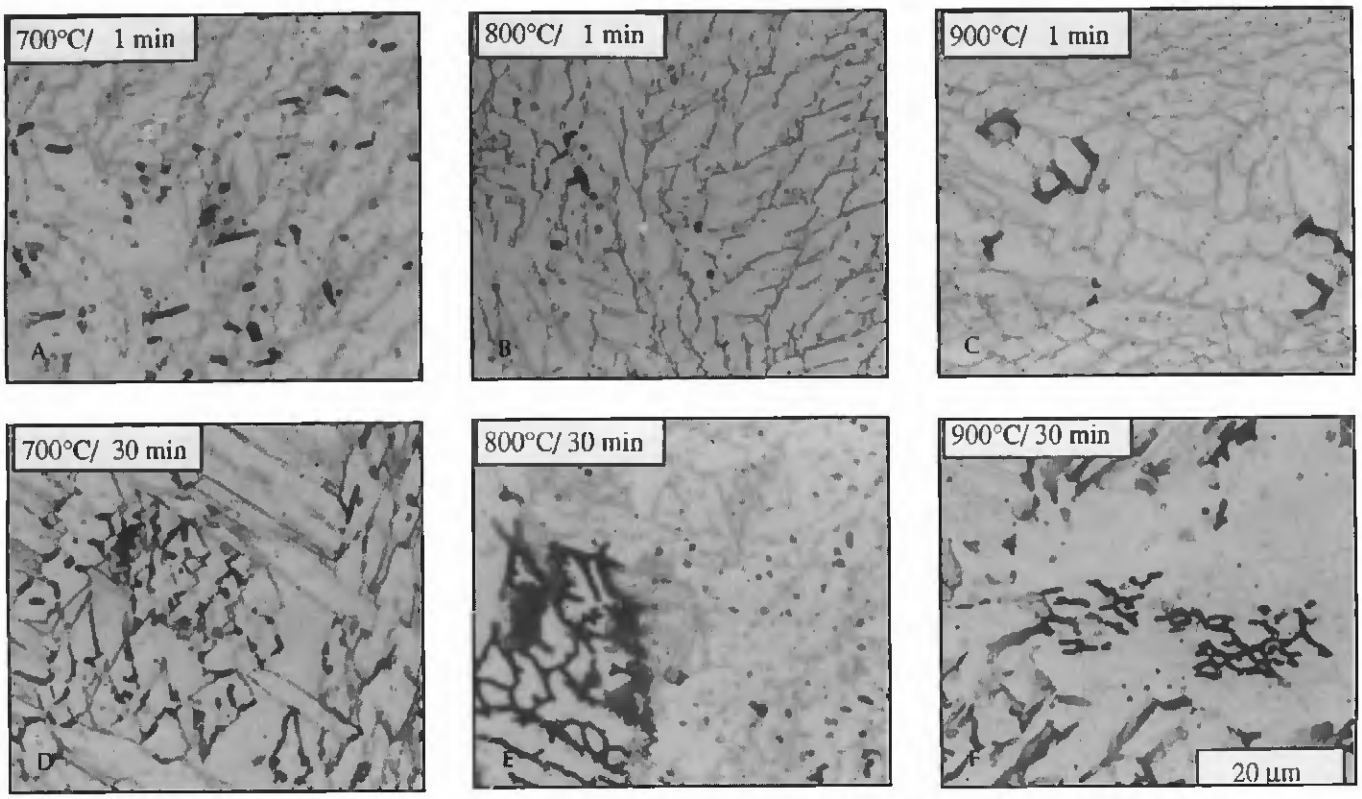

Fig. 16 — Light optical micrographs showing the microstructure of the heat treated OK 67.50 weld metal after oxalic acid etching. Precipitates are etched preferentially and give a dark contrast. Small precipitates appear already after aging for 1 min at 700° or 800°C and are frequent after 30 min aging. Only larger precipitates are found after heat treatment at 900°C. Large precipitates appear also after 30 min aging at 800°C (cf. Fig. 2).

Table 6 — Ferrite Content, Room-Temperature Impact Toughness and Hardness

Heat treatment	Ferrite content (FN)	Impact toughness (J)	Hardness (HV_{10})
OK 67.50			
As-welded	30	50	256
700°C/1 min	28	63	272
700°C/30 min	29	59	278
700°C/3 h	16	8	272
800°C/1 min	26	66	272
800°C/5 min	24	25	274
800°C/30 min	17	11	292
800°C/3 h	1	2	322
900°C/1 min	24	51	258
900°C/5 min	21	18	262
900°C/30 min	11	4	295
900°C/3 h	1	3	311
950°C/30 min	7	3	294
1000°C/30 min	20	12	261
Exp. rutile			
As-welded	35	—	—
675°C/1 h	29	—	—
800°C/30 min	22	—	—
Exp. basic			
As-welded	33	112	—
675°C/1 h	28	—	—
800°C/30 min	14	—	—

the basic weld metal.

Both the absolute corrosion rates and the increase after heat treatment was higher in the Huey test than in the Streicher test. No attempt was made to perform Huey testing on the specimens heat treated at 800°C due to the very high corrosion rates found after heat treatment at 675°C.

Discussion

Precipitation Reactions

Three different intermetallic phases and $M_{23}C_6$-carbides were identified. A previously not reported feature in 22%Cr duplex weld metals is the formation of grain boundary films. R- and σ-phase were the most frequently occurring precipitates; whereas, χ-phase was found only for one aging temperature. Other secondary phases (τ-phase, Cu-particles, M_7C_3, π- phase, Cr_2N and CrN) have earlier been identified in duplex stainless base metals and weld metals (Refs. 4, 10). However, none of these were detected, neither by TEM nor by x-ray diffraction. Some of these phases (M_7C_3, Cr_2N and CrN) might have been present although in too small volume fractions to be detected. The low Cu content (<0.1%) makes it unlikely that Cu-particles would precipitate and τ- and π- phases have only been reported for aging at 600°C or below. R- and σ-phase were clearly the only two phases present in sufficient quantities to be of practical importance for mechanical properties and those most influencing the corrosion resistance.

Intermetallic Phases

The measured compositions of σ- and χ-phase (Table 4) are in good agreement with those reported in literature (Refs. 3, 6, 13 and 24). The situation is more complex for R-phase. This intermetallic phase has earlier been found in duplex weld metals and duplex and super-duplex stainless base metals aged between 550° and 700°C (Refs. 2, 4, 5, 7, 10, 13, 16). In a 22%Cr duplex weld metal, R-phase with

a composition of 24%Fe 25%Cr 5%Ni 40%Mo 5%Si formed at grain boundaries; whereas, R-phase that formed intragranularly contained 32%Fe 25%Cr 5%Ni 34%Mo 4%Si (Refs. 13, 14).

The Mo-content of the small R-phase particles (Table 4) found after aging at 675°, 700° or 800°C increased with increasing temperature (27, 36 and 39 %, respectively); whereas, the Cr-content decreased (30, 22 and 16–20%, respectively). The Cr-content also decreased with longer aging times. The compositions fall in the same range as those reported for the intra- and intergranular R-phase formed at 600°C, although they differ in details (Refs. 13, 14). However, in the present study, the composition of R-phase did not vary for a given heat treatment condition. This could be taken as an indication that the location of precipitation is of less importance for the composition at higher temperatures. The differences in composition are probably connected to the change in the ferrite composition induced by the formation of Cr-rich σ-phase. Furthermore, R-phase nucleated and grew quickly but was replaced by σ-phase after longer aging times. Obviously σ-phase is the more stable phase after long aging times (Ref. 10).

The situation for R-phase is further complicated by the presence of larger R-phase particles with a higher Cr and a lower Mo content. Large R-phase particles were found after aging at 700°C for 3 h or at 800°C for 30 min. These are the two heat treatments at which the largest volume fractions of R-phase had formed and substantial amounts of σ-phase were present. It is possible that the larger R-phase is favored by the change in ferrite composition induced by σ-phase precipitation. However, this needs to be verified by further investigation. It is clear, though, that the composition of R-phase can vary considerably depending on formation temperature, size, ferrite composition and location of precipitation.

The rate of precipitation was significantly lower in the basic experimental weld metal than in the other two weld metals. As seen in Table 5, the partitioning of elements between ferrite and austenite was smaller for the basic than for the rutile weld metal, but the ferrite levels were similar (Table 6). Therefore, the differences in precipitation rates can be explained by differences in alloying content of the ferrite (Ref. 15).

Grain Boundary Films

An unexpected finding was the presence of seemingly continous films, with a composition (Table 5) close to that of R-phase, on many ferrite/austenite boundaries in the experimental weld metals heat treated at 675°C. Little information exists in the literature about grain boundary films in duplex base metals or weld metals (Ref. 9). However, very thin, probably icosahedral, intermetallic (26%Fe 30%Cr 37%Mo 3.5%Si) films have been found upon aging of a 20%Cr 10%Ni 2.6%Mo duplex base metal at 400° or 550°C (Ref. 25). "Laminate-shaped" grain boundary precipitates have been reported to form in 18%Cr 5%Ni 3%Mo duplex stainless base metals during aging in the temperature range 450°–750°C (Ref. 26). These precipitates formed most rapidly at 600°C and had a composition corresponding to $Fe_3Cr_3Mo_2Si_2$ (29%Fe 27%Cr 34%Mo 10%Si). No attempt was made to identify their structure. Another candidate that cannot be ruled out from the composition is π-nitride. However, the absence of N-enrichment at grain boundaries, evidenced by SIMS studies (Fig. 13), and the absence of separate π-phase precipitates makes this phase less likely.

With the presently available information, it is not possible to identify the grain boundary films. Furthermore, it is not known whether this film is stable for longer aging times. However, it seems that grain boundary films are most likely to form at temperatures below 700°C for longer aging times. Therefore, the importance of the grain boundary films in connection with welding is probably small in comparison with that of other precipitates.

Carbides and Nitrides

Apart from intermetallic phases, carbides and nitrides have also been identified in duplex stainless base metals and weld metals (Refs. 4, 6, 27). Only a few $M_{23}C_6$ carbides and no nitrides were found by TEM, x-ray diffraction and SIMS. The carbides were mainly found in the experimental basic weld metal which has a higher C-content than the other two weld metals.

π-phase nitride was the only type of carbide or nitride present in sufficient quantities to be detected by TEM after 24-h aging of a 22%Cr 8%Ni 3%Mo weld metal at 600°C (Ref. 13). A complementary x-ray diffraction study of extracted residue showed that also minor amounts of $M_{23}C_6$ carbides and Cr_2N nitrides were present. However, Nilsson, *et al.* (Ref. 13), concluded that the volume fractions of these phases were extremely small and of no practical importance. Contrarily, in a recent study on 22%Cr duplex stainless base metals with C-contents similar to those of the OK 67.50 and the rutile experimental weld metal, AEM showed that $M_{23}C_6$ carbides and Cr_2N nitrides were present in detectable amounts already after 1–3 min (Ref. 6). Cr_2N formed most quickly around 850°C and $M_{23}C_6$ most quickly around 800°C.

Table 7 — Corrosion Rate in Streicher and Huey Tests (mm/year)

Condition	As-welded	675°C/ 1 h	800°C/ 30 min
Streicher test			
Experimental rutile	0.27	2.1	6.1
Experimental basic	0.24	0.8	2.6
Huey test			
Experimental rutile	0.45	15	—
Experimental basic	0.30	5.6	—

There seems to be a significant difference between the importance of $M_{23}C_6$ or Cr_2N precipitation in duplex stainless base metals and weld metals for similar C- and N-contents. This difference can most probably be explained by the lower ferrite content of the weld metal, resulting in a lower C and N concentration in the austenite, and the weld metal ferrite morphology with a large fraction of planar, coherent phase boundaries being less effective nucleation sites for precipitation. In conclusion, carbide and nitride precipitation appear to be insignificant compared to precipitation of intermetallic phases in duplex weld metals.

Mechanical Properties

Even though σ-phase formed large precipitates and increased the hardness significantly; whereas, R-phase formed smaller precipitates and affected hardness less, the effect on impact toughness was similar for both phases. The impact toughness dropped drastically when 3–5 vol-% of intermetallic phases had formed — Table 6. A similar effect on impact toughness has also been reported for the duplex steel SAF 2205 where the presence of approximately 4 vol-% σ-phase decreased the toughness to unacceptable levels (Ref. 24).

The embrittlement occurs more rapidly in the weld metal compared to the corresponding duplex base metal (UNS S31803, W.Nr 1.4462). The impact toughness of the weld metal has decreased to below the commonly used acceptance level of 27 J after approximately 3 to 4 min at 850° to 950°C (Fig. 17); whereas, the base metal, depending on starting condition, will be embrittled after 10 to 40 min (Refs. 1, 3, 24, 28). However, the time to embrittlement

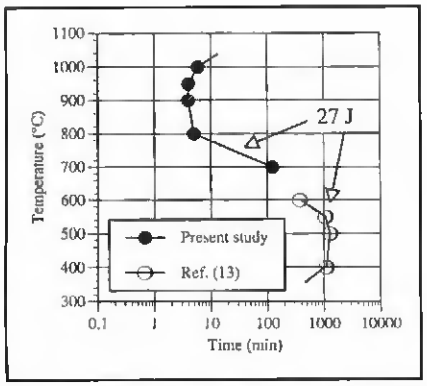

Fig. 17 — Critical aging time for embrittlement at room temperature of a 22Cr-9Ni-3Mo-0.15N type duplex weld metal.

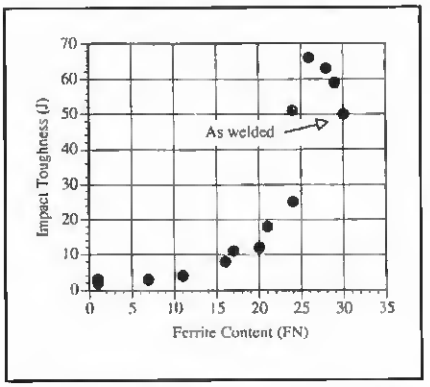

Fig. 18 — Correlation between impact toughness and ferrite content for heat treated 22Cr-9Ni-3Mo-0.15N type duplex weld metal.

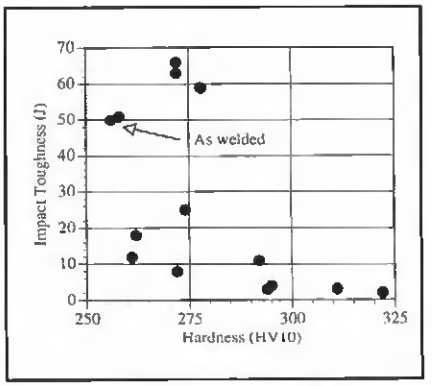

Fig. 19 — Impact toughness vs. hardness for heat treated 22Cr-9Ni-3Mo-0.15N-type duplex weld metal.

leaves a broad margin for the cooling rates normally obtained with recommended welding procedures. It should also be pointed out that the critical times determined here are conservative since "a worst case" weld metal with a large fraction of reheated (and multiply reheated) regions was studied. Consequently, the time to start of embrittlement (1 min around 900°C) found in this study is somewhat shorter than that reported in another study on 22%Cr duplex weld metals (1.5 min) (Ref. 12).

Ferrite Content, Hardness and Impact Toughness

A significant decrease in ferrite content or an increase in hardness clearly indicated serious embrittlement by precipitation of intermetallic phases — Table 6, Figs. 18, 19. For example, the impact toughness had in all cases decreased to below 12 J when the average hardness was above 290 HV_{10} or the average ferrite content was below 20 FN.

Changes in ferrite content and hardness can be used as tools to identify serious embrittlement but not to guarantee the absence of embrittlement — Figs. 18, 19. For example, the hardness after 5 min aging at 900°C was 262 HV_{10} compared to 256 HV_{10} as welded. Nevertheless, the impact toughness had decreased to 18 J. Furthermore, the ferrite content was 24 FN after 5 min at 800°C or after 1 min at 900°C, but the impact toughness was 25 J in the first case and 51 J in the second. That impact toughness is affected before a hardness increase is detected is in line with the finding that precipitation of approximately 2% of σ-phase is needed to give a clearly noticeable effect on hardness (Refs. 7, 29).

Corrosion Resistance

When discussing the influence of intermetallic phases the main concern is usually the effects on mechanical properties (Refs. 4, 12, 13, 24). However, it is well known that the presence of intermetallic phases will also deteroriate the corrosion resistance, and that the effect on corrosion resistance of small amounts of precipitates is stronger than the effect on mechanical properties (Ref. 30). Little information is available about the relative importance of different intermetallic phases and all intermetallic phases are, therefore, generally treated as being equally deleterious (Refs. 1, 4, 6, 31).

Oxalic Acid Test

In the oxalic acid etch test, stainless steels are polarized to a highly positive potential in the very transpassive range. In this potential range, the corrosion rate increases with increasing Cr-content and precipitates rich in Cr and Mo are preferentially dissolved (Ref. 31). The observed etching behavior of the heat treated specimens is in good agreement with that expected from the composition of the different phases. The dissolution rate was lowest for the austenite, having the lowest Cr- and Mo-content and highest for the Cr- and Mo-rich precipitates.

Two temperature regimes can be distinguished when plotting the approximate time for significant etching attack in the oxalic acid test on the TTT-diagram for R- and σ-phase precipitation (Fig. 20). At 800° and 900°C the oxalic acid attack curve closely follows the curve for σ-phase precipitation. However, at 700°C significant etching attack was found already after 1 min; whereas, 1% R-phase was estimated to have formed after approximately 1 h. The appearance of the etching attack was the same for all heat treatment times at 700°C.

A somewhat different etching behavior has been observed for 22%Cr duplex stainless base metals. Significant etching attack was found after 3 min aging temperatures in the range 650° to 900°C, but no intermediate temperature where etching attack was displaced to longer times was observed (Ref. 27). The etching attack in the upper part of this temperature range was attributed to σ- and χ-phase precipitation; whereas, the etching attack at lower temperatures was considered to be an effect of nitride and carbide precipitation.

Carbide or nitride precipitation seems to be a less likely explanation of the etching behavior below 800°C in the weld metal. Several observations suggest that rapid nucleation of R-phase formation is more probable. No local etching at grain boundaries was seen in the weld metal and no carbides and nitrides were detected in the OK 67.50 weld metal. Furthermore, the most rapid precipitation of carbides and nitrides would be expected above 700°C; whereas, oxalic etching produced a more significant etching attack after 1 min aging at 700°C than after aging at 800°C. Therefore, carbide and nitride precipitation must be either insignificant or occur simultaneously as precipitation of intermetallic phases in the weld metal. Anyhow, the effect on corrosion resistance must be small compared to the effect of intermetallic precipitates.

Consequently, the TTT-diagram for R-phase precipitation (Fig. 20) describes the time to formation of larger volume fractions of R-phase (>1%) correctly; whereas, the curve showing the time to significant attack in oxalic acid more accurately describes the time to start of of R-phase formation. Therefore, the TTT-diagram (Fig. 11) can be used to predict the risk of embrittlement; whereas, the curve showing significant oxalic acid attack (Fig. 20) shows when effects on corrosion can be expected. It can be noted that the times allowed at elevated temperatures before significant attack in oxalic acid oc-

curs are of the same order for duplex base metals and weld metals (1–5 min).

Streicher and Huey Test

As described in the ASTM A 262 standard, the presence of σ-phase will cause high corrosion rates in Huey and Streicher tests (Ref. 20). Therefore, the high corrosion rates for the experimental weld metals heat treated at 800°C are reasonable since both σ–phase and R-phase had formed. There was also a clear correlation between the amount of precipitates and corrosion rate, as can be seen from the higher corrosion rate of the rutile experimental weld metal, which showed the more extensive precipitation.

The high corrosion rates when only R-phase was present after aging at 675°C, show that the Huey and Streicher tests also detect R-phase in duplex weld metals. This is in agreement with the high corrosion rates in the Huey test caused by other Mo-rich intermetallic phases, like Laves and χ-phase (Refs. 1, 31).

Ferrite Content, Hardness and Corrosion Resistance

It is interesting to note that corrosion resistance and toughness will start to deteroriate almost simultaneously during aging above 800°C, whereas corrosion resistance will be affected after significantly shorter times than toughness after heat treatment below 800°C. The reason is that small amounts of precipitates will give a more significant effect on corrosion resistance than on toughness. Therefore, a significant decrease in ferrite content or an increase in hardness, compared to the as welded condition, should be taken as an indication of a seriously lowered corrosion resistance — Table 6 and Fig. 20. However, the same approach cannot be used to guarantee an unaffected corrosion resistance.

Welding in Practice

Embrittlement during holding at elevated temperatures occurs somewhat more rapidly in the weld metal compared to in the corresponding duplex base metal (Refs. 1, 3, 24, 28). However, oxalic acid etching shows that the time before the corrosion resistance will start to deteroriate is similar for the base metal and the weld metal. The weld metal will not be a weak link in this respect. Practical experience verifies that lowered corrosion resistance due to slow cooling after welding, of 22%Cr duplex base metals and weld metals, is very uncommon. Quite contrarily, any corrosion problems in connection to welding are most often due to nitride precipitation caused by overly rapid cooling or caused by poor gas protection of the root in one-sided welding (Ref. 12). Therefore, the present investigation and practical experience show that embrittlement or loss of corrosion resistance will not occur in the weld metal when recommended welding procedures are followed. Also, repair welding can normally be performed without risk of weld metal embrittlement.

Conclusions and Summary of Results

Precipitation of intermetallic phases in the temperature interval 675°–1000°C (1247°–1832°F) and its effects on corrosion resistance and impact toughness were studied for 22%Cr 9%Ni 3%Mo 0.15%N-type duplex weld metals. The following conclusions were reached:

1) The intermetallic phases σ-, R- and χ-phase formed during aging. Only σ- and R- phases were present in sufficient quantities to affect mechanical properties.

2) R-phase was the major phase precipitating at 675° and 700°C (1247° and 1292°F); whereas, σ–phase replaced R-phase after longer aging times at 800°C (1472°F) and was the only phase found after aging at higher temperatures. Some χ-phase formed at 800°C (1472°F).

3) Two types of R-phase appeared. Small particles (10–100 nm) and after longer aging times also larger particles (≈0.5 μm).

4) Continuous grain boundary films appeared after aging at 675°C (1247°F).

5) R-phase formed rapidly around 700°C (1292°F) but had a low growth rate compared to σ–phase.

6 Only minor amounts of carbides were found in the experimental weld metals. No nitrides were detected.

7) Typical compositions as measured by EDX-analysis were: σ–phase: 55%Fe, 34%Cr, 4%Ni, 6%Mo, 1%Si; small R-phase: 33-38%Fe, 16-30%Cr, 3-5%Ni, 27-39%Mo, 3-4%Si; large R-phase: 36-43%Fe, 25-26%Cr, 3-4%Ni, 25-26%Mo, 2-3%Si; G. b. film: 26%Fe, 33%Cr, 3%Ni, 33%Mo, 3%Si; χ-phase: 49%Fe, 28%Cr, 3%Ni, 18%Mo, 1-2%Si

8) The impact toughness dropped below 27 J when 3–5 vol-% of intermetallic phases had formed. The decrease in impact toughness was most rapid between 850°–950°C.

9) Significant etching attack in the oxalic acid test was found for aging times from 1 min at 900°C (1652°F), from 5 min at 800°C (1472°F) and from 1 min at 700°C (1292°F). The attack was due to σ–phase precipitation after aging at and above 800°C; whereas, etching after aging at 700°C was caused by rapid formation of R-phase.

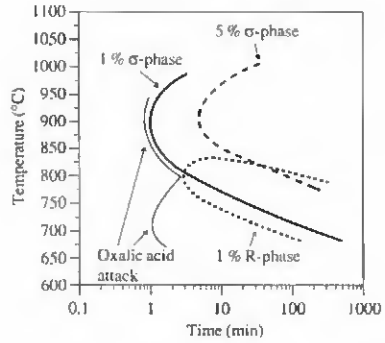

Fig. 20 — Time for significant attack in oxalic acid superimposed on TTT diagram for R- and σ–phase precipitation in a 22Cr-9Ni-3Mo-0.15N type duplex weld metal.

10) Huey and Streicher testing was sensitive to R- and σ-phase precipitation in duplex weld metals.

11) Corrosion resistance and toughness will deteroriate almost simultaneously during aging above 800°C (1472°F); whereas, corrosion resistance will be affected before toughness at lower temperatures.

12) Embrittlement during holding at elevated temperatures occurs somewhat more rapidly in 22%Cr duplex weld metals than in base metals; whereas, the time to start of deteroriation of corrosion resistance is similar for base metals and weld metals.

13) A significant decrease in ferrite content or an increase in hardness indicated serious embrittlement and lowered corrosion resistance due to precipitation of intermetallic phases. However, ferrite content or hardness cannot be used to guarantee an unaffected corrosion resistance or the absence of embrittlement.

14) Embrittlement or loss of corrosion resistance will not occur in the weld metal if recommended welding procedures are followed.

Acknowledgments

Ms. L. Boström and Ms. A.-C. Gustavsson are thanked for skillful specimen preparation. Comments on the manuscript by the authors colleges at The Esab Group R & D departments are gratefully acknowledged.

References

1. Herbsleb, G., and Schwaab, P. 1983. Proc. Conf. Duplex Stainless Steels '82, ed. Lula, R. A., ASM International, Materials Park, Ohio, pp. 15–40.

2. Solomon, H. D., and Devine, T. M. *ibid.*, pp. 693–756.

3. Thorvaldsson, T., Eriksson, H., Kutka, J., and Salvén, A. 1984. Proc. Conf. Stainless Steels '84, The Institute of Metals, London, pp. 101–105.

4. Josefsson, B., Nilsson, J.-O. and Wilson, A. 1991. Proc. Conf. Duplex Stainless Steels '91, eds. Charles, J., and Bernhardsson, S., *Les Éditions de Physique*, Les Ulis Cedex A, France, pp. 67–78.

5.Redjaïmia, A., Metauer, G., and Gantois, M. *ibid.*, pp. 119–126.

6. Hertzman, S., Lehtinen, B., Symniotis–Barrdahl, E. 1992. Proc. Conf. Applications of Stainless Steels '92, eds. H. Nordberg and J. Björklund, Jernkontoret, Stockholm, Sweden, pp. 345–359.

7. Nilsson, J.-O., Wilson, A., Josefsson, B., and Thorvaldsson, T. ibid, pp. 280–289.

8. Wahlberg, G. 1989. The role of nitrogen in duplex stainless steels, Ph.D. dissertation. Chalmers Univ. Techn., Göthenburg, Sweden.

9. Guttman, M. 1991. Proc. Conf. Duplex Stainless Steels '91, eds. J. Charles, and S. Bernhardsson, *Les Éditions de Physique*, Les Ulis Cedex A, France, pp. 79–92.

10.Nilsson, J.O. 1992. Mater. Sci. Techn., 8 (8): 685–700.

11. Kotecki., D. J. 1989. *Welding Journal* 68 (11): 431-s to 441-s.

12. Van Nassau, L., Meelker, H., and Hilkes, J. 1991. Proc. Conf. Duplex Stainless Steels '91, eds. Charles, J., and Bernhardsson, S., *Les Éditions de Physique*, Les Ulis Cedex A, France, pp 303–323.

13. Nilsson, J.O., and Liu, P. 1991. Mater. Sci. Techn., 7 (9): 853–862.

14. Nilsson, J.O., and Liu, P. 1991. Proc. Conf. Stainless Steels '91, The Iron and Steel Institute of Japan, Tokyo, pp. 1109–1116.

15. Karlsson, L., and Pak, S. 1991. Proc. Conf. Stainless Steels'91, The Iron and Steel Institute of Japan, Tokyo, pp. 1101–1108.

16. Karlsson, L., Ryen, L., Rolander, U., and Pak, S. Proc. Conf. Applications of Stainless Steels '92, eds. H. Nordberg, and J. Björklund, Jernkontoret, Stockholm, Sweden, pp. 335–344.

17. Karlsson, L., and Pak, S. Proc. Conf. Corr. of Welded Constr. and Pressure Vessels, Centro Nacional de Investigaciones Metalurgicas, Madrid, Spain, pp. 13–24.

18. American Welding Society. 1991. ANSI/AWS A4.2-91, AWS, Miami, Florida.

19. Vander Voort, G. F. 1989. J O M 41 (3): 6–11.

20. American Society for Testing and Materials, ASTM A262-85, Annual book of ASTM Standards, ASTM, Philadelpia, Pa.

21. Hall, E. O., and Algie, S. H. 1966. Metall. Rev. 11: 61.

22. Rideout, S., Manley, W. D., Kamen, E. L., Lement, B. S., and Beck., P. A. 1951. Trans. AIME. 191: 872–876.

23. Kasper., J. S. 1954. Acta Met. 2: 456–461.

24. Jackson, E. M. L. E. M., and Matthews, L. M. 1991. Proc. Conf. Stainless Steels '91, The Iron and Steel Institute of Japan, Tokyo, pp. 730–737.

25. Auger, P., Danoix, F., Menand, A., Bonnet, S., Bourgoin, J., and Guttman, M. 1990. Mater. Sci. Techn. , 6 (3): pp 301-313.

26. Shiying, Lu. 1984. Proc. Conf. Stainless Steels '84, The Institute of Metals, London, pp. 106–113.

27. Honglu, C., and Hertzman, S. 1991. Internal Report No 2689, Swedish Institute for Metals Research, Stockholm, Sweden.

28. Norberg, P. 1986. Proc. Conf. Duplex Stainless Steel '86, Nederlands Institute voor Laastechniek, The Hague, The Netherlands, pp. 298–302.

29. Maderud, C.-J., Andersson, J.-O., and Liljas, M. 1992. Proc. Conf. Applications of Stainless Steels '92, eds. Nordberg, H., and Björklund, J., Jernkontoret, Stockholm, Sweden, pp. 370–378.

30. Karlsson, L., Pak, S., and Andersson, S. L. *ibid.*, pp. 1093–1100.

31. Herbsleb, G., and Schwaab, P. 1986. *Werkstoffe und Korrosion*. 37 (1): 24–35.

JOINING OF 6061 ALUMINUM MATRIX-CERAMIC PARTICLE REINFORCED COMPOSITES

By R. Klehn and T. W. Eagar

The joining of 6061 aluminum reinforced with 15 volume percent Al_2O_3 was studied. Transient liquid phase bonding with silver, copper and aluminum-12 atomic percent silicon were the three systems which demonstrated an ability to join the aluminum-based composite. The physical phenomena controlling transient liquid phase bonding of aluminum alloys were also examined to gain a better understanding of the joining processes.

The study of each joint included a shear test, metallographic and compositional examination of the joint, and tensile tests of the strongest braze systems.

Publication of this document was sponsored by the Welding Research Council, Inc.

The price of WRC ***Bulletin 385 (September 1993)*** is $45.00 per copy, plus $5.00 for U.S. and Canada, or $10.00 for overseas, postage and handling. Orders should be sent with payment to the Welding Research Council, Inc. • 345 E. 47th St. • Room 1301 • New York, NY 10017 • (212) 705-7956.